Research Paper
J. Astron. Space Sci. 39(2), 67-77 (2022)
https://doi.org/10.5140/JASS.2022.39.2.67

JASS Journal of Astronomy and Space Sciences

Interaction of Ion Cyclotron Electromagnetic Wave with Energetic Particles in the Existence of Alternating Electric Field Using Ring Distribution

Kumari Neeta Shukla[1], Jyoti Kumari[2], Rama Shankar Pandey[2†]

[1]Department of Applied Sciences, Manav Rachna International Institute of Research and Studies, Faridabad , Haryana, 121001, India
[2]Department of Physics, Amity Institute of Applied Sciences, Amity University, Noida, Uttar Pradesh 201303, India

The elements that impact the dynamics and collaborations of waves and particles in the magnetosphere of planets have been considered here. Saturn's internal magnetosphere is determined by substantiated instabilities and discovered to be an exceptional zone of wave activity. Interchanged instability is found to be one of the responsible events in view of temperature anisotropy and energization processes of magnetospheric species. The generated active ions alongside electrons that constitute the populations of highly magnetized planets like Saturn's ring electron current are taken into consideration in the current framework. The previous and similar method of characteristics and the perturbed distribution function have been used to derive dispersion relation. In incorporating this investigation, the characteristics of electromagnetic ion cyclotron wave (EMIC) waves are determined by the composition of ions in plasmas through which the waves propagate. The effect of ring distribution illustrates non-monotonous description on growth rate (GR) depending upon plasma parameters picked out. Observations made by Cassini found appropriate for modern study, have been applied to the Kronian magnetosphere. Using Maxwellian ring distribution function of ions and detailed mathematical formulation, an expression for dispersion relation as well as GR and real frequency (RF) are evaluated. Analysis of plasma parameters shows that, proliferating EMIC waves are not developed much when propagation is parallelly aligned with magnetosphere as compared to waves propagating in oblique direction. GR for the oblique case, is influenced by temperature anisotropy as well as by alternating current (AC) frequency, whereas it is much affected only by AC frequency for parallel propagating waves.

Keywords: magnetosphere of Saturn, electromagnetic ion cyclotron waves, dispersion relation, ring distribution function, method of characteristics

1. INTRODUCTION

Saturn is known to have a pronounced plasma and radio wave emission system (Gurnett et al. 1981, 2005; Kurth & Gurnett 1991) like other outer planets such as Jupiter, Uranus, Neptune, and also the earth, reflecting the global view of magnetospheric dynamics. These emissions are completely characterized by non-thermal features of particle distribution in velocity space (i.e., $\partial f/\partial \mathbf{v}_{\|} > 0$). Stochastic processes and instabilities generated within the magnetosphere could be considered as a response mechanism for these emissions, which are influenced by the particle species available in the magneto plasma and magnetospheric forces. Saturn consists of charged particles with versatile energy ranges and neutral from various satellites and ionospheres of giant planets and the solarfields wind. When these charged particles interact with the wave propagating within the magnetosphere, they can exchange energy and momentum and thus the wave can grow. The major contributor, Enceladus, used Saturn's

Received 08 MAR 2022 **Revised** 11 APR 2022 **Accepted** 28 APR 2022
†**Corresponding Author**
Tel: +91-986-863-9418, E-mail: rspandey@amity.edu
ORCID: https://orcid.org/0000-0003-4907-1080

http://janss.kr pISSN: 2093-5587 eISSN: 2093-1409

magnetic properties to fill magnetosphere of Saturn. Some unbiased species are contemplated to be ionized through accuse trade of magnetospheric plasma, sun oriented intense UV radiation and electron impact. These recently created particles move at the Kepler speed and later speed up to (nearly) the Saturn corotation velocity. The primary driver of this speed increase is E × B floats along the cycloidal direction introducing temperature anisotropy in ions participating in transportation around. The low ion frequency (i.e., $f < fc_i$) was found to be associated with the watery component (H_2O). Additionally, these electromagnetic ion cyclotron wave (EMIC) waves can be polarized in both the sense as right and left-handed waves and can get affected in the presence of heavy ions (He^+, O^+ & N^+) (Mauk 1982). EMIC Waves have been extensively reported in Jupiter (Kivelson & Southwood 1996), Saturn (Smith & Tsurutani 1983) and also in comets (Lee 1989) and are believed to be existed in the region where total pressure prevails magnetic pressure. The rate of ion production can be estimated by using the amplitude of the EMIC wave (Huddleston & Johnstone 1992; Cowee et al. 2009) and Loss rate (Hansen et al. 2006; Leisner et al. 2006).

The Wave-Particle Interaction Mechanism – contributes a lot in space and is believed to be of utmost importance mainly in the emergence of the magnetopause boundary layer, auroras, radio wave emissions, energization process etc. Electric and magnetic field components of the wave can exasperate the directions of the particles by scattering them due to their interaction with charged particles within the magnetosphere. The significant outcome of Wave-particle interaction (WPI) takes place only when particle have a cyclotron resonance with wave i.e., There must have a comparable frequency of the wave with one or more of the three occasional motions of the particle (i.e., gyro, drift and bounce), driving the infringement of adiabatic invariants (Thorne 2010). This interaction may lead to energization, landau damping etc. like processes causing damping / growth of wave. Generation of plasma wave instability is another outcome of the interplay between wave and particles where wave enhancement or damping can cause particles to lose or gain energy accordingly (considering their relative velocities). Kennel & Petschek (1966) explained well the (wave-WPI) in view of growth of waves in a very subtle way. Evidence of acceleration and scattering losses as a consequence of WPI is also well demonstrated by Summers et al. (2007). Discussion on WPI outcome is limited here as the study is focused on generation of EMIC is also wave near the equatorial plane.

EMIC wave can be influenced in presence of heavy ions and these waves are classified in three prime frequency band range: Helium 'He^+', hydrogen 'H^+' and oxygen 'O^+', found to be most abundant (Meredith et al. 2014), excitation of which depends on the availability of species (i.e., hot & cold) in the magnetosphere. Remarkable inward radial diffusion of hot components found an extensive event causing 'growth' of the ion cyclotron wave (ICW). The event (mixing of hot and cold components) permits an exceptional source of energy-yielding pressure (thermal) anisotropies ($T_\perp > T_\parallel$) of energetic ions (up to few electron volts to thousand electron volts i.e., 10 eV–100 KeV) (Summers & Thorne 2003). Preceding research revealed that the EMIC waves are excited more often in day-side (specifically post noon to dusk) regions (Usanova et al. 2013) due to the blending of the old component from the plasmasphere and hot component of ring.

It is observed that EMIC wave propagating bidirectional (in both the bearings of the equatorial plane i.e., South and north) and ascertained a narrow band (with the thickness of ± 0.1 R_s) near Saturn equatorial plane, manifesting the Doppler shift (Leisner et al. 2011). Two different maxima's (peaks) in the power spectrum have been found in such a bidirectional region; this layer was interpreted as a wave generation region and found to propagate in the northward and southward direction of the equatorial wave generation region.

At Saturn's magnetosphere, the perpendicular corotation speed of drifted plasma influences ions generated from neutrals of the icy moon and are taken up into ring distributions which are unstable to grow ion waves of low frequency.

The inner magnetospheric plasma correlates with Saturn (Wilson et al. 2009) and thus the neutral particles emitted by Enceladus move significantly faster at their local Kepler velocity. Many pioneers demonstrated how the convective electric field (the injection velocity) relates to the difference between magnetospheric plasma bulk velocity and neutral particles Keplerian velocity. This is evident that a ring distribution is created by absorbed ions in velocity space (e.g., Coates 2004).

2. RING DISTRIBUTION AND SATELLITE'S FLYBYS

The ring distribution of ions is unstable to produce a low-frequency ion cyclotron (left-handed polarized wave) just below the local ion frequency. It is observed that the newly born ions (due to the ionization process) get fully integrated into the flow of Saturn ambient magnetospheric plasma as process showing the conversion of ring distribution into a shell-like distribution and then into Maxwellian distribution

by significant velocity diffusion (Szegö et al. 2000; Cowee et al. 2009). All three Pioneer 11 (1979), Voyager 1 (1980), and Cassini (2004–2017) reported ICW in the magnetosphere of Saturn. Pioneer, 11 vector helium magnetometer, has given the extensive view on ICW within inner magnetosphere in close proximity of Dione lying at 6 L.

Prior studies recommended the pickup of oxygen ions as a source of these EMIC waves generated near the equatorial plane. Additionally, Barbosa (1993) determined the ion cyclotron wave, originated due to temperature anisotropy in the near-equatorial region from radial distance 5 R_s to 7 R_s using data from Voyager 1, showing a similar band of frequencies (close to the gyrofrequency of O^+), Rodríguez-Martínez et al. (2010) also confirmed ICW and harmonics generated due to temperature anisotropies within the middle magnetosphere. Many pioneer investigators reported the generation of 'Ion cyclotron wave' in the intrinsic Saturn environment (Leisner et al. 2006; Rodríguez-Martínez et al. 2010; Meeks et al. 2016).

Consequently, in our present work, we dissected the development pace of EMIC waves along the equatorial plane of Saturn. As referenced before, there are numerous species of particles and wave connections in Saturn's magnetospheric plasma (Frank et al. 1980), statistical techniques have been found more advantageous to introduce a macroscopic depiction of the plasma wonder. The kinetic method and drift kinetics method were developed by Lee & Kaw (1972) and were utilized by Inhester (1990), showing that the outrageous growth rate (GR) is diminished because of warm impacts. This underlines the requirement of Kinetic approach to treat issues. To characterize plasma instability conditions and GR, we used kinetic approximations given by Brinca & Tsurutani (1989a, b). Thorne & Summers (1989) used the analytical method to best study the wave-excited linear phase. Driven by the above literature, the current evaluation has been employed to obtain the dispersion relation wherever the dependency of wave growth is governed by dimensionless integration using a ring distribution function. In the case of Saturn's relativistic effects, ion cyclotron instability plays a crucial role in wave-WPIs (Summers et al. 2007). Therefore, we introduce a relativistic effect in the equation to enhance the time GR. Studies show that the lower wave number spectra are affected by the loss cone distribution of particles and these waves increase till 1° (Kumari et al. 2018). Many pioneers such as Pandey et al. (2008), Pandey & Singh (2010) etc. have studied characteristics of EMIC waves using kinetic approach by distribution functions like kappa distribution and generalized distribution. Based on previous literature, this work has been further extended to the ring distribution effect on ion cyclotron waves.

3. EMPIRICAL DISPERSION MODEL

Electric and magnetic fields have direction along the z-axis, with magnitude $B = B_o\hat{e}_z$ and EF $E = E_0 \sin \nu t\hat{e}_z$ is presumed in the environment of an anisotropic, homogeneous, and collision-less plasma. Inhomogeneity over micro scale is supposed to have in interaction zone in this specifically.

The involvement of the Vlasov equation helped us reach the perturb state of particles (avoiding higher -order terms), deriving perturbed trajectories of particles alongside bothered conveyance work. Conductivity tensor and dispersion relation for a relativistic case with an effective AC EF for n = 1, have been derived here. The method is completely linear and analogous to the technique used by Kumari & Pandey (2019) and Shukla et al. (2021).

Thus, using eq^n 9 given by Kumari & Pandey (2019), Dielectric tensor is given as:

$$\varepsilon_{ij}(k,\omega) = 1 + \sum_s \frac{4e_s^2\pi}{(\beta m_s)^2 \omega^2} \sum_n \sum_p J_p(\lambda_2) \int \frac{\|S_{ij}^*\| d^3p}{\omega - \frac{k_\| p_\|}{\beta m_e} - \frac{k_\| \Gamma_z}{\beta \nu} + p\nu - \frac{n\omega_c}{\beta}} \quad (1)$$

Where, β is the relativistic factor and is defined as $1/\sqrt{1-\frac{v^2}{c^2}}$. For propagation of electromagnetic waves, the general dispersion relation reduces to $\varepsilon_{11} \pm i\varepsilon_{12} = N^2$ where $N^2 = \frac{k^2c^2}{\omega^2}$. The dispersion relation for the relativistic case with parallel AC EF is written as:

$$\frac{k^2c^2}{\omega^2} = 1 + \sum_s \frac{4e_s^e\pi}{(\beta m_s)^2 \omega^2} \sum J_p(\lambda_2) \int \frac{d^3p}{2} p_\perp \left[\begin{array}{l} (\beta m_s)\left(\omega - \frac{k \| p \|}{\beta m_s}\right)\frac{\partial f_o}{\partial p_\perp} \\ -k_\| (\beta m_s)\frac{\partial f_o}{\partial p_\perp}\frac{\Gamma_z}{\beta\nu}\left(\frac{p}{\lambda_2} - 1\right) \\ +k_\| p_\perp \frac{\partial f_o}{\partial p_\|} \end{array} \right] \times \left(\frac{1}{\omega - \frac{k \| p \|}{\beta m_s} - \frac{k \| \Gamma_z}{\beta \nu} + p\nu \pm \frac{\omega_c}{\beta}} \right) \quad (2)$$

where, subscript s' denotes type of species i.e., electrons and ions. The ring distribution function is assumed to be the distribution function of the trapped particles (Wu et al. 1989; Kumari & Pandey 2018).

$$f\left(p_{\perp},\mathrm{p}_{||}\right)=\frac{n_s/\mathrm{n}}{\pi^{3/2}p_{o||s}p_{o\perp s}^{2}A}\exp\left[-\frac{\left(p_{\perp}-v_o\right)^2}{p_{o\perp s}^{2}}-\frac{\left(p_{||}^{2}\right)}{p_{o||s}^{2}}\right] \quad (3)$$

$$A=\exp\left(-\frac{v_o^2}{p_{o\perp s}^{2}}\right)+\sqrt{\pi}\left(\frac{v_o}{p_{o\perp s}}\right)\mathrm{erfc}\left(-\frac{v_o}{p_{o||s}}\right) \quad (4)$$

where $p_{o||e}=\left(k_bT_{||e}/\beta m_e\right)^{1/2}$, $p_{o\perp e}=\left(k_bT_{\perp}/\beta m_e\right)^{1/2}$, $p_{o||i}=\left(k_bT_{||i}/\beta m_i\right)^{1/2}$ and $p_{o\perp i}=\left(k_bT_{\perp i}/\beta m_i\right)^{1/2}$, are the associated parallel and perpendicular thermal momenta of electrons and ions respectively. $\mathrm{n_s}$ / n, in Eq. (3) represents the ratio of particle total density captured and characterized by high energy, and erfc(x) in Eq. (4) is a complementary error function. The drift velocity is represented as v_0.

Substituting $d^3p=2\pi\int_0^{\infty}p_{\perp}\mathrm{d}p_{\perp}\int_{-\infty}^{\infty}\mathrm{d}p_{||}$ and using expression (2) in Eq. (1) and after solving the integrations, we get the dispersion relation as:

$$\frac{\mathrm{k^2c^2}}{\omega^2}=1+\frac{4e_s^2\pi}{\left(\beta\mathrm{m_s}\right)^2\omega^2}\sum_p J_p\left(\lambda_2\right)\frac{\left(\mathrm{n_s/n}\right)}{\mathrm{A}}\left(\beta m_s\right)\left[\frac{\beta m_s}{p_{o||s}}\left(\frac{\omega}{k_{||}}-\frac{\Gamma_{||s}}{\beta\nu}\left(\frac{p}{\lambda_2}-1\right)\right)\mathrm{X_1Z}\left(\xi\right)+\mathrm{X_2}\left(1+\xi\mathrm{Z}\left(\xi\right)\right)\right] \quad (5)$$

The above dispersion relation is now approximated in the ion cyclotron range of frequencies.

Electron's temperature is assumed to be $\mathrm{T}_{\perp e}=\mathrm{T}_{\parallel e}=\mathrm{T}_e$ and magnetised with, $\left|\omega_r+i\gamma\right|\ll\omega_{ci}$.

Whereas ions are assumed to have the condition $T_{\perp i}>\mathrm{T}_{\parallel i}$ and $\left|k_{\parallel}p_{o||i}\right|\ll\left|\omega_r\pm\frac{\omega_{ci}}{\beta}+i\gamma\right|$.

So, considering these approximations, Eq. (5) becomes:

$$D(k,\omega_r+i\gamma)=1-\frac{k^2c^2}{\left(\omega_r+i\gamma\right)^2}+\sum_p J_p\left(\lambda_2\right)\left[\begin{array}{l}\left(\frac{\omega_{pe}^2}{\omega_{ci}^2}-\frac{\omega_{pe}^2}{\left(\omega_r+i\gamma\right)\left(\pm\omega_{ci}\right)}\right)X_{1e}\left(\beta m_e\right)\\ +\frac{\omega_{pi}^2}{\left(\omega_r+i\gamma\right)^2}\left(\begin{array}{l}X_{1i}\frac{\left(\beta m_i\right)}{p_{o||i}}\left(\frac{\omega_r+i\gamma}{k_{\parallel}}-\frac{\Gamma_{||i}}{\beta\nu}\left(\frac{p}{\lambda_2}-1\right)\right)Z\left(\xi_i\right)\\ +X_{2i}\left(1+\xi_iZ\left(\xi_i\right)\right)\end{array}\right)\end{array}\right] \quad (6)$$

where,

$$X_{1i}=1+\frac{v_o^2}{p_{o\perp i}^2}-\sqrt{\pi}\frac{v_o}{p_{o\perp i}},\ X_{1e}=1+\frac{v_o^2}{p_{o\perp e}^2}-\sqrt{\pi}\frac{v_o}{p_{o\perp e}}$$

and

$$X_{2i}=X_{1i}+\frac{p_{o\perp i}^2}{p_{o||i}^2}\left(1-\sqrt{\pi}\frac{v_o^3}{p_{o\perp i}^3}erfc\left(\frac{v'_{\perp i}}{p_{o\perp i}}\right)+3\frac{v_o^2}{p_{o\perp i}^2}-\frac{3}{2}\sqrt{\pi}\frac{v_o}{p_{o\perp i}}\right)$$

After using the charge neutrality condition $\frac{\omega_{pe}^2}{\pm\omega_{ce}^2}=\frac{-\omega_{pi}^2}{\pm\omega_{ci}^2}$ and the condition $\left|\frac{k^2c^2}{\omega^2}>>1+\frac{\omega_{pe}^2}{\omega_{ce}^2}\right|$ Dispersion relation reduces to -

$$D\left(k,\omega_r+i\gamma\right)=-\frac{k_{\parallel}^2c^2}{\omega_{pi}^2}+\sum_p J_p\left(\lambda_2\right)\left[\begin{array}{l}\frac{\omega}{\pm\omega_{ci}}\left(\beta m_e\right)X_{1e}\\ +\left(\beta m_i\right)X_{1i}\left\{\begin{array}{l}\frac{\beta m_i}{p_{o||i}}\left(\frac{\omega}{k_{\parallel}}-\frac{\Gamma_{||i}}{\beta\nu}\left(\frac{p}{\lambda_2}-1\right)\right)Z\left(\xi_i\right)\\ +\frac{X_{2i}}{X_{1i}}\left(1+\xi_iZ\left(\xi_i\right)\right)\end{array}\right.\end{array}\right] \quad (7)$$

Now the function $Z\left(\xi\right)=\frac{1}{\sqrt{\pi}}\int_{-\infty}^{\infty}\frac{e^{-t^2}}{t-\xi}\mathrm{d}t$, stands for plasma dispersion where,

$$\xi=\frac{\beta m_i\omega-\frac{k_{||}\Gamma_{||s}m_i}{\nu}+\left(\beta m_i\right)p\nu\pm m_i\omega_c}{k_{||}p_{o||i}}$$

$\omega_{pi}^2=\frac{4\pi e^2}{\left(\beta m_i\right)^2}\frac{n_i/n}{B}$ Now the function $Z\left(\xi\right)=\frac{1}{\sqrt{\pi}}\int_{-\infty}^{\infty}\frac{e^{-t^2}}{t-\xi}\mathrm{d}t$, stands for plasma dispersio.

Now, dimensionless parameter wave vector $\tilde{k}=\frac{k_{||}p_{o||i}}{\omega_{ci}}$ is introduced.

3.1 Case I

In the parallel direction to magnetic field, real frequency and GR are expressed as:

$$\frac{\gamma}{\omega_{ci}}=\frac{\frac{\sqrt{\pi}}{\tilde{k}}\left(\frac{X_{2i}}{X_{1i}}-k_4\right)k_3^3\exp\left[-\left(\frac{k_3^2}{\tilde{k}}\right)^2\right]}{1+\frac{\tilde{k}^2}{2k_3^2}+\frac{\tilde{k}^2}{k_3}\left(\frac{X_{2i}}{X_{1i}}-k_4\right)+\frac{m_e}{m_i}\frac{X_{1e}}{X_{1i}}k_3^2} \quad (8)$$

The real part of Eq. (8) is

$$X_3=-\frac{\beta\omega_r}{\omega_c}=X_4+\frac{\tilde{k}^2}{2\beta_1}\left[\frac{X_{2i}}{X_{1i}}\frac{\beta_1}{\left(1+X_4\right)}-\frac{\left(1+X_4\right)}{\beta X_{1i}}\right] \quad (9)$$

Where $k_3=1-\beta X_3+\beta X_4$, $k_4=\frac{\beta X_3-\beta X_4}{1-\beta X_3+\beta X_4}$ and

$$\beta_1 = \frac{4\pi\mu_o\varepsilon_o k_b T_{||i}\left(n_i / n\right)}{AB_o^2},\ X_4 = \frac{k_{||}\Gamma_{||i}}{\beta\nu\omega_c} - \frac{p\nu}{\omega_c} \quad (10)$$

3.2 Case II

In the oblique direction to magnetic field, real frequency and GR are expressed as:

$$\frac{\gamma}{\omega_{ci}} = \frac{\frac{\sqrt{\pi}}{\tilde{k}\cos\theta}\left(\frac{X_{2i}}{X_{1i}} - k_4\right)k_3^3 \exp\left[-\left(\frac{k_3^2}{\tilde{k}\cos\theta}\right)^2\right]}{1 + \frac{\left(\tilde{k}\cos\theta\right)^2}{2k_3^2} + \frac{\left(\tilde{k}\cos\theta\right)^2}{k_3}\left(\frac{X_{2i}}{X_{1i}} - k_4\right) + \frac{m_e}{m_i}\frac{X_{1e}}{X_{1i}}k_3^2} \quad (11)$$

The real part of Eq. (11) is

$$X_3 = -\frac{\beta\omega_r}{\omega_c} = X_4 + \frac{\left(\tilde{k}\cos\theta\right)^2}{2\beta_1}\left[\frac{X_{2i}}{X_{1i}}\frac{\beta_1}{\left(1+X_4\right)} - \frac{\left(1+X_4\right)}{\beta X_{1i}}\right] \quad (12)$$

4. RESULTS AND DISCUSSION

4.1 Important Magnetospheric Parameters

To analyse the enhancement rate of EMIC wave at 5 R_s (the region of peak density), influenced by ring distribution in the Saturn inner magnetosphere, given plasma parameters have been considered. An extensive survey of Saturn plasma electron environment done by Sittler et al. (1983) in view of Voyager flybys. An EF E_o = 0.01 mV/m, electron density (n_o) =5 × 10^6 m^{-3}. Though electron densities are found to be extremely variable (decreasing with increasing radial distances) between 3 R_s to 9 R_s due to centrifugal outward transport of plasma, evaluated by Persoon et al. (2005) using Cassini data and ambient magnetic field B_o = 184 nT has been taken into account. The range of alternating current (AC) frequency for background plasma is 4 Hz to 12 Hz and temperature anisotropy A_T is assumed to change from 0.25 to 0.75. Barbosa (1993) reported variance in temperature anisotropy (from 1 to 3) due to an anisotropic distribution of pickup O^+ ions in the intrinsic magnetosphere, causing wave growth with peak amplitude ~2 nT near the equatorial plane in the view of Voyager 1 observation. Young et al. (2005) and Rymer et al. (2007) have done substantial studies on colder (Approx. less than 100 ev) and hotter (Approx. greater than 100 ev) components to be radially diffused outward and inward, respectively, in respect of centrifugally-oriented instability (Interchanging of these components through transportation) and energy-specific penetration. $K_BT_{||}$ is taken to be 200 eV for background electrons depicting thermal energy and 1 keV for isotropic energetic ions (Pandey et al. 2008).

4.2 Parallel and Oblique Propagation

Fig. 1(a) Depicts the variation in GR for parallel traversing ion waves with respect to the magnetic field for numerous values of 'AC frequency' (υ) versus 'wave number' ($\tilde{k}$). The GR γ / ω_c = 0.145 is achieved at $\tilde{k}$ (0.42) for υ = 4 Hz. For the value of alternating frequency υ = 8 Hz, the maxima appear to be shifted towards $\tilde{k}$ = 0.44 with γ / ω_c = 0.169. When υ increased to 12 Hz, maximum GR is achieved i.e., γ / ω_c = 0.183 at $\tilde{k}$ (0.46). In the case of GRs, the spread of the spectrum at lower frequencies is accompanied by a peak shift from 0.42 to 0.46 (due to the Doppler shift resonance

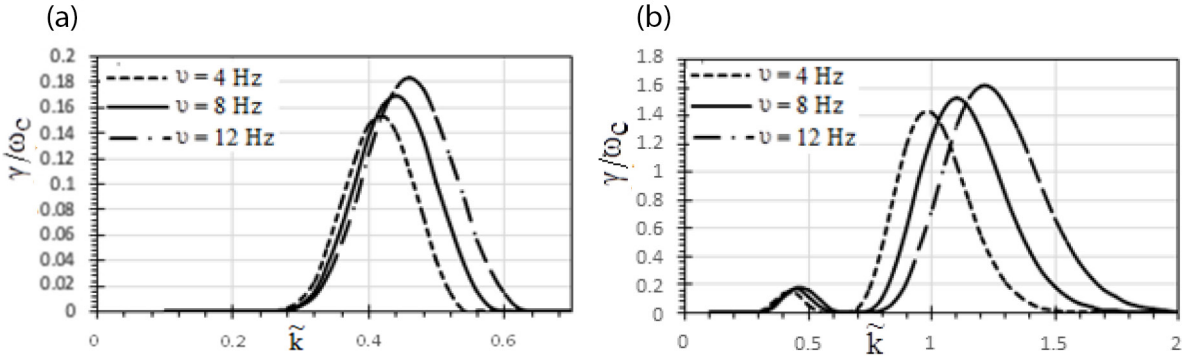

Fig. 1. Growth rate for parallel and oblique propagation for AC frequency. (a) Parallel propagation: Change in growth rate with respect to $\tilde{k}$ for numerious values of AC frequency under constant values such as temperature anisotropy, number density. (b) Oblique propagation: Change in growth rate with respect to $\tilde{k}$ for numerious values of AC frequency under constant values such as temperature anisotropy, number density (Graph corrected). AC, alternating current.

condition) occurring in the Saturn magnetosphere. Fig. 1(b) considers oblique propagation of waves and shows variation for different AC frequency values. As it is evident from the graphs that oblique propagation of ion cyclotron waves gives rise to first and second order harmonics. The first harmonics occur at γ / ω_c = 0.178, 0.169, and 0.141 with constant values of wavenumber $\tilde{k}$ (0.45), for increasing frequencies from 4 Hz to 12 Hz, which is approximately close to the magnitude of GR for parallel propagating EMIC waves. However, the second harmonics arise at an extremely higher wavenumber side with an enhanced peak GR. The value of the maximum peak appears at γ / ω_c = 1.425 for υ = 12 Hz at $\tilde{k}$ (1.2). The peak seems to be shifted to the lower wavenumber side from $\tilde{k}$ (1.2) to $\tilde{k}$ (1) as AC frequency decreases to 8 Hz, then to 4 Hz. The contribution of the AC frequency reduces the upper limit of the wave number. This indicates that the presence of a minimum of the parallel AC field frequency is sufficient to trigger instability of the ion cyclotron. The results are consistent with the normalized GR of the ion cyclotron wave of the perpendicular AC field considered in the magnetosphere (Pandey & Singh 2010).

Fig. 2(a) and 2(b) shows the change in the GR of different pressure (temperature) anisotropy values with respect to the wave number for parallel propagation. In above derivation term '$T_\perp / T_\parallel$' equate $A_T + 1$. Thus, for pressure anisotropy $T_\perp / T_\parallel$ (1.25), the maximum G. R. γ / ω_c = 0.165. For pressure anisotropy $T_\perp / T_\parallel$ (1.5), GR γ / ω_c = 0.169. Similarly, for pressure anisotropy $T_\perp / T_\parallel$ (1.75), the GR γ / ω_c = 0.171. For most of the pressure (temperature) anisotropy values, the maxima appear at $\tilde{k}$ (0.44). Conclusively, as a ratio of temperatures, $T_\perp / T_\parallel$ increases, and when a wave propagates parallel to the ambient magnetic field, the GR of the EMIC wave increases. Earlier discussed parallel case does not indicate ample variation, but temperature anisotropy is supposed to promote oblique propagation as second harmonics appear at greater γ / ω_c along with wide bandwidth spectrum. This propagation shows its highest peak at 1.611 for $\tilde{k}$ (1.15) and enhances as the value of temperature anisotropy increases. It can be said that the temperature anisotropy enhances the GR by acting as a source of energy. For ions, EMIC waves are thought to act as whistler waves as on electrons. Thus, temperature anisotropy is considered to be the foremost source of free energy to the plasma.

Fig. 3(a) shows the change in the GR for parallel propagating waves to magnetic fields with respect to $\tilde{k}$ for various values of the relativistic factor β. For β = 0.5 and β = 0.6, γ / ω_c = 0.169 and γ / ω_c = 0.161 at $\tilde{k}$ (0.44) and $\tilde{k}$ (0.43) respectively and at β (0.7), γ / ω_c = 0.157 at $\tilde{k}$ (0.42) has been calculated. The corresponding $\tilde{k}$ value maxima shift from 0.44 to 0.42. As the propagation of waves is changed to oblique, the growth of waves shows double harmonics. However, Fig. 3(b) studies oblique propagation of EMIC waves. Broadening of the wave spectrum and shift to lower wave numbers for higher values of the relativistic factor is clearly visible in the graph. Although in this case also, second harmonics peaked to higher GR under same conditions. For relativistic factor β = 0.5, first peak occurs at γ / ω_c = 0.169 for $\tilde{k}$ (0.45) and second peak appear at γ / ω_c = 1.526 for $\tilde{k}$ (1.1). Similarly, for β = 0.6 and 0.7, second harmonics appears at γ / ω_c = 1.491 and γ / ω_c = 1.454 with $\tilde{k}$ (1.05) and $\tilde{k}$ (1) respectively. Thus, the above figures, it can be inferred that the relativistic factor does not support growth of waves. Kumari et al. (2019) also quoted similar results for whistler-mode waves. Therefore, the higher s the energy of the particles, the smaller is the magnitude of the relativistic factor causing more ion cyclotron wave growth.

Fig. 4(a) and 4(b) show the varying GR of ion cyclotron

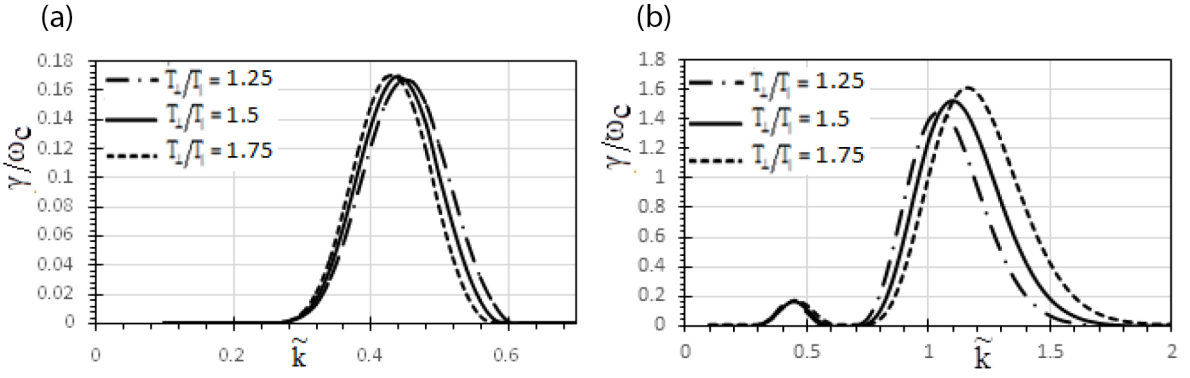

Fig. 2. Growth rate for parallel and oblique propagation for perpendicular to parallel temperature ratio. (a) Parallel propagation: Change in growth rate with respect to $\tilde{k}$ for numerous values of temperature anisotropy under constant values of AC frequency, number density etc. (b) Oblique propagation: Change in growth rate with respect to $\tilde{k}$ for numerous values of temperature anisotropy under constant values of AC frequency, number density etc. AC, alternating current.

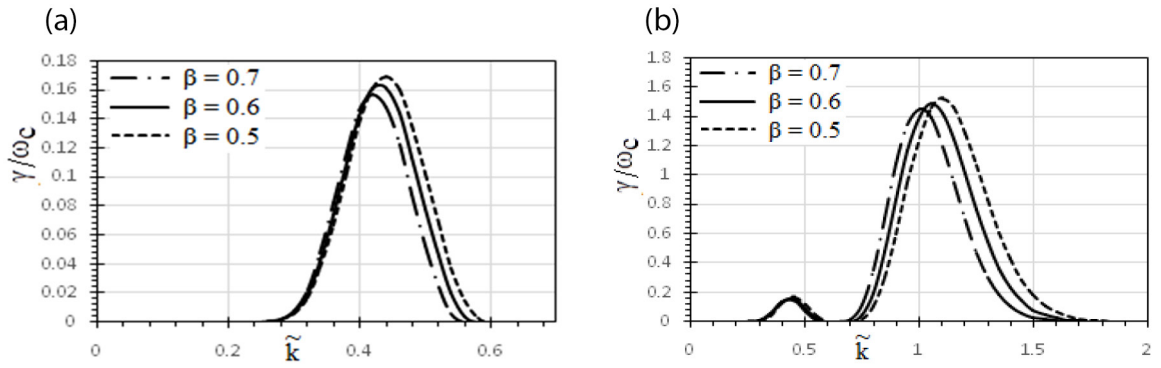

Fig. 3. Growth rate for parallel and oblique propagation for relativistic factor. (a) Parallel propagation: Change in growth rate with respect to $\tilde{k}$ for numerous values of relativistic factor under constant values of AC frequency, temperature anisotropy, number density etc. (b) Oblique propagation: Change in growth rate with respect to $\tilde{k}$ for numerous values of relativistic factor under constant values of AC frequency, temperature anisotropy, number density etc. AC, alternating current.

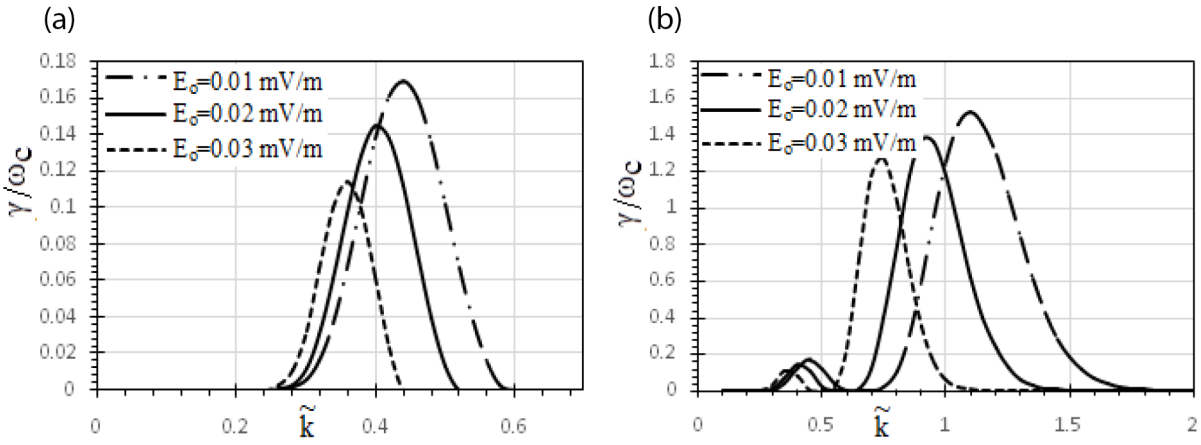

Fig. 4. Growth rate for parallel and oblique propagation for magnitude of electric field. (a) Parallel propagation: Change in growth rate with respect to $\tilde{k}$ for numerous values of electric field amplitude under constant values of AC frequency, temperature anisotropy, number density etc. (b) Oblique propagation: Change in growth rate with respect to $\tilde{k}$ for numerous values of electric field amplitude under constant values of AC frequency, temperature anisotropy, number density etc. AC, alternating current.

instability at various E_o values. We can deduce by seeing the figure that when we study the ring distribution in the magnetosphere of Saturn, the enhancement in EF strength does not promote the growth of the electromagnetic ion cyclotron instability, and it is in the whistler case where Loss cone distribution support the unstable acoustic modes (Kumari et al. 2018). Similar results were shown when the ion cyclotron wave was studied using particle analysis by Ahirwar et al. (2006). Second-order harmonics are also discussed in this study. It can be said that higher-order harmonics affect higher WN (wavenumber) spectra. Fig. 4(b) shows the variation of the oblique propagation of the wave and inferred that the GR is significantly affected by the change in the amplitude of the EF and widens the higher wavenumber side.

Fig. 5. Explicating the GR of EM ion cyclotron waves for numerous values of pitch angle (PA) (θ, angle of propagation) of wave. As PA increases, the GR is found to be increased more (from 0.169 to 0.171) for the first harmonics, as the PA ranges from 1o to 3o alongside shifting of $\tilde{k}$ (from 0.45 to 0.5). A very minute comparative study has been done by Blanco-Cano et al. (2001a, b), showing maximum growth for $AC_{\parallel}$ EFs with increased wave number. Hence, the graph also shows second harmonics with the highest peak values as $\gamma / \omega_c = 1.596$ for $3o\theta$, $\gamma / \omega_c = 1.556$ for $2\theta o$ and $\gamma / \omega_c = 1.526$ for $1\theta o$ at $\tilde{k}$ (1.25, 1.15, and 1.1) respectively. Cowley et al. (2006) have also reported a greater GR for parallel propagation in comparison to oblique, when examining obliquely propagating ion cyclotron waves produced due to ionization of neutrals coming about in pickup particles in Saturn's magnetosphere.

Fig. 6(a) and 6(b) show the graph for the GR of ion

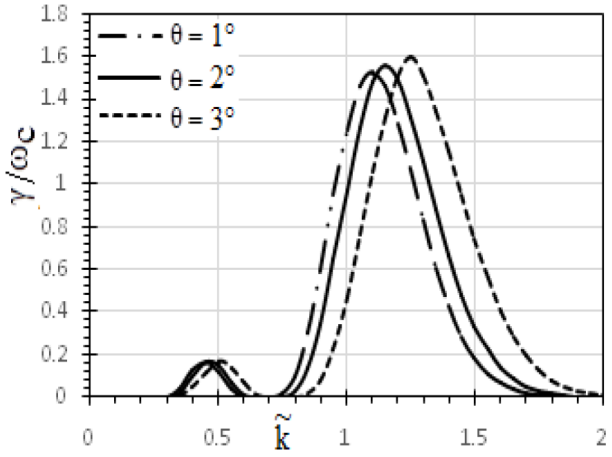

Fig. 5. Oblique propagation: Change in growth rate with respect to $\tilde{k}$ for numerous values of angle of propagation under constant values of AC frequency, temperature anisotropy, number density. etc. AC, alternating current.

cyclotron waves versus wave number for different values of ion density. In Fig. 6(a), for parallel propagation, GR has been plotted against ion number density –3 × 10^7 m^{-3}, 5 × 10^7 m^{-3}, and 7 × 10^7 m^{-3}. It can be seen that γ / ω_c = 0.196, 0.175, and 0.173 at $\tilde{k}$ (0.48, 0.46, and 0.44) respectively. In Fig. 6(b), for oblique propagation, the GR changes from 1.708 to 1.551 while evolving higher ion density from 3 × 10^7 m^{-3} to 7 × 10^7 m^{-3} with shifting of wave-number towards lower side i.e., 1.35 to 1.15 thus decreasing the wavenumber indicating the occurrence of multiple harmonics at the same instant. Therefore, as the ion number density in plasma systems increases, the GR of ion cyclotron waves decreases. Ion number density is related to ion plasma frequency and it is also related to the mass of the ion, which is greater than the electron. Electromagnetic ion cyclotron wave ions dominate. Conclusion made is analogous to the analysis done by Kumari & Pandey (2018).

5. CONCLUSION

EMIC waves are believed to be responsible to invoke ion acceleration in magnetic layers and usually observed on the auroral channels of the terrestrial magnetosphere (Ashour-Abdalla & Thorne 1978; Kintner et al. 1978; Lysak et al. 1980), of Jupiter (Cowley & Bunce 2001) and of Saturn observed by HST and Cassini during high latitude pass. These can be found far away from the reason source. The heating effect of ions could also be understood in terms of free energy source (Mitchell et al. 2009) within Saturn. The physical origin of these auroras is yet to be understood in all outer planets. In this framework, considering the ring distribution, oblique (very low angle) and parallel propagation of electromagnetic ion cyclotron waves is reviewed. Using the linear dispersion relation, the expression of the GR of the wave and magnetic field interacting with the wave is derived. Result analysis depicts enhanced GR for greater temperature anisotropy and it is also found to be elevated with increased AC frequency, but GR seems not to be much affected for parallel propagation. It is also being observed that the extent of the EF, relativistic factor does not favour GR. As $\beta = 1/\sqrt{1-\frac{v^2}{c^2}}$, if velocity of energetic particles is more, magnitude of the relativistic factor will be reduced inferring more wave growth i.e., particles with more energy will contribute more to grow as compared to the particle of lesser energy. Hence for higher β, GR found to be decreased. This study is based on the wave-WPI and transformation of energy from the particles to wave and growth of wave has been analysed

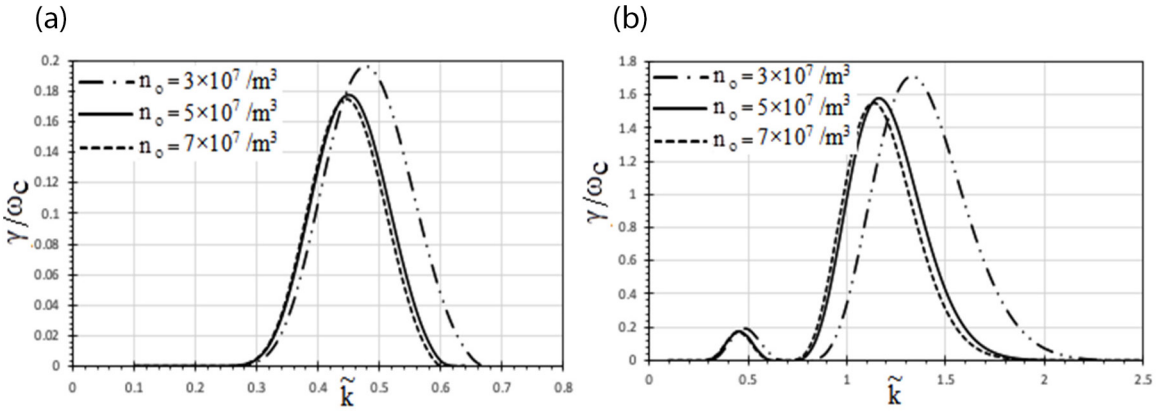

Fig. 6. Growth rate for parallel and oblique propagation for ion density. (a) Parallel propagation: Change in growth rate with respect to $\tilde{k}$ for numerous values of ion density under constant values of AC frequency, temperature anisotropy etc. (b) Oblique propagation: Change in growth rate with respect to $\tilde{k}$ for numerous values of ion density under constant values of AC frequency, temperature anisotropy etc. AC, alternating current.

rigorously. Observing the EMIC wave interaction with ring particles in magnetosphere of Saturn near equator, it is seen that as the wavenumber increases, the bandwidth raises towards higher wavenumber side, and the GR attains the highest peak with increasing value of temperature anisotropy. Therefore, it can be inferred that electromagnetic ion cyclotron instability assuming the ring distribution of particles, affects the spectra's greater wave numbers and gives rise to second harmonics for oblique propagation. Inequality in magnitude of maximum GR is also observed i.e., GR for parallel propagation shows slightly smaller value than the oblique propagation for each condition.

The study mainly concerns about grown waves linked with the distribution of energetic ions and electrons within Saturn inner magnetosphere and could bring significant conceptual developments in the mechanism of generation method (reflecting magnetospheric local processes and complex structure), involving various parameters causing GR and can put forward to evaluate various instabilities, compositional evaluation and scattering losses (as also suggested inside 6 L by Leisner et al. 2006, Rymer et al. 2007) in a different magnetospheric plasma environment including comets. More substantial analysis of EMIC wave origin remains for future investigation.

ACKNOWLEDGMENTS

Authors are grateful to the reviewers of paper for their expert comments and evaluating the manuscript fastidiously.

ORCIDs

Kumari Neeta Shukla https://orcid.org/0000-0001-6076-1678
Jyoti Kumari https://orcid.org/0000-0001-5611-5286
Rama Shankar Pandey https://orcid.org/0000-0003-4907-1080

REFERENCES

Ahirwar G, Varma P, Tiwari MS, Electromagnetic ion-cyclotron instability in the presence of a parallel electric field with general loss-cone distribution function - particle aspect analysis, Ann. Geophys. 24, 1919–1930 (2006). https://doi.org/10.5194/angeo-24-1919-2006

Ashour-Abdalla M, Thorne RM, Toward a unified view of diffuse auroral precipitation, J. Geophys. Res. 83, 4755-4766 (1978). https://doi.org/10.1029/JA083iA10p04755

Barbosa DD, Theory and observations of electromagnetic ion cyclotron waves in Saturn's inner magnetosphere, J. Geophys. Res. Space Phys. 98, 9345-9350 (1993). https://doi.org/10.1029/93JA00476

Blanco-Cano X, Russell CT, Strangeway RJ, The Io mass-loading disk: wave dispersion analysis, J. Geophys. Res. Space Phys. 106, 26261-26275 (2001a). https://doi.org/10.1029/2001JA900090

Blanco-Cano X, Russell CT, Strangeway RJ, Kivelson MG, Khurana KK, Galileo observations of ion cyclotron waves in the Io torus, Adv. Space Res. 28, 1469-1474 (2001b). https://doi.org/10.1016/S0273-1177(01)00548-8

Brinca AL, Tsurutani BT, On the excitation of cyclotron harmonic waves by newborn heavy ions, J. Geophys. Res. Space Phys. 94, 5467-5473 (1989a). https://doi.org/10.1029/JA094iA05p05467

Brinca AL, Tsurutani BT, The oblique behavior of low-frequency electromagnetic waves excited by newborn cometary ions, J. Geophys. Res. Space Phys. 94, 3-14 (1989b). https://doi.org/10.1029/JA094iA01p00003

Coates AJ, Ion pickup at comets, Adv. Space Res. 33, 1977-1988 (2004). https://doi.org/10.1016/j.asr.2003.06.029

Cowee MM, Omidi N, Russell CT, Blanco-Cano X, Tokar RL, Determining ion production rates near Saturn's extended neutral cloud from ion cyclotron wave amplitudes, J. Geophys. Res. Space Phys. 114, A04219 (2009).

Cowley SWH, Bunce EJ, Origin of the main auroral oval in Jupiter's coupled magnetosphere–ionosphere system, Planet. Space Sci. 49, 1067-1088 (2001). https://doi.org/10.1016/S0032-0633(00)00167-7

Cowley SWH, Wright DM, Bunce EJ, Carter AC, Dougherty MK, et al., Cassini observations of planetary-period magnetic field oscillations in Saturn's magnetosphere: Doppler shifts and phase motion, Geophys. Res. Lett. 33, L07104 (2006). https://doi.org/10.1029/2005GL025522

Frank LA, Burek BG, Ackerson KL, Wolfe JH, Mihalov JD, Plasmas in Saturn's magnetosphere, J. Geophys. Res. Space Phys. 85, 5695-5708 (1980). https://doi.org/10.1029/JA085iA11p05695

Gurnett DA, Kurth WS, Hospodarsky GB, Persoon AM, Averkamp TF, et al., Radio and plasma wave observations at Saturn from Cassini's approach and first orbit, Science 307, 1255-1259 (2005). https://doi.org/10.1126/science.1105356

Gurnett DA, Kurth WS, Scarf FL, Plasma waves near Saturn: initial results from Voyager 1, Science 212, 235-239 (1981). https://doi.org/10.1126/science.212.4491.235

Hansen CJ, Esposito L, Stewart AIF, Colwell J, Hendrix A, et al., Enceladus' water vapor plume, Science 311, 1422-1425 (2006). https://doi.org/10.1126/science.1121254

Huddleston DE, Johnstone AD, Relationship between wave

energy and free energy from pickup ions in the comet halley environment, J. Geophys. Res. Space Phys. 97, 12217-12230 (1992). https://doi.org/10.1029/92JA00726

Inhester B, A drift-kinetic treatment of the parametric decay of large-amplitude Alfven waves, J. Geophys. Res. Space Phys. 95, 10525-10539 (1990). https://doi.org/10.1029/JA095iA07p10525

Kennel CF, Petschek HE, Limit on stably trapped particle fluxes, J. Geophys. Res. 71, 1-28 (1966). https://doi.org/10.1029/JZ071i001p00001

Kintner PM, Kelley MC, Mozer FS, Electrostatic hydrogen cyclotron waves near one Earth radius altitude in the polar magnetosphere, Geophys. Res. Lett. 5, 139-142 (1978). https://doi.org/10.1029/GL005i002p00139

Kivelson MG, Southwood DJ, Mirror instability II: the mechanism of nonlinear saturation, J. Geophys. Res. Space Phys. 101, 17365-17371 (1996). https://doi.org/10.1029/96JA01407

Kumari J, Kaur R, Pandey RS, Effect of hot injections on electromagnetic ion-cyclotron waves in inner magnetosphere of Saturn, Astrophys. Space Sci. 363, 33 (2018). https://doi.org/10.1007/s10509-018-3250-0

Kumari J, Pandey RS, Study of VLF wave with relativistic effect in Saturn magnetosphere in the presence of parallel A.C. electric field, Adv. Space Res. 63, 2279-2289 (2019). https://doi.org/10.1016/j.asr.2018.12.013

Kumari J, Pandey RS, Whistler mode waves for ring distribution with A.C. electric field in inner magnetosphere of Saturn, Astrophys. Space Sci. 363, 249 (2018). https://doi.org/10.1007/s10509-018-3466-z

Kurth WS, Gurnett DA, Plasma waves in planetary magnetospheres, J. Geophys. Res. Space Phys. 96, 18977-18991 (1991). https://doi.org/10.1029/91JA01819

Lee MA, Ultra-low frequency waves at comets, in plasma waves and instabilities at comets and in magnetospheres, eds. Tsurutani BT, Oya H (American Geophysical Union, Washington, DC, 1989), 13-29.

Lee YC, Kaw PK, Parametric instabilities of ion cyclotron waves in a plasma, Phys. Fluids 15, 911 (1972). https://doi.org/10.1063/1.1693999

Leisner JS, Russell CT, Dougherty MK, Blanco-Cano X, Strangeway RJ, et al., Ion cyclotron waves in Saturn's E ring: initial cassini observations, Geophys. Res. Lett. 33, L11101 (2006). https://doi.org/10.1029/2005GL024875

Leisner JS, Russell CT, Wei HY, Dougherty MK, Probing Saturn's ion cyclotron waves on high-inclination orbits: lessons for wave generation, J. Geophys. Res. Space Phys. 116, A09235 (2011). https://doi.org/10.1029/2011JA016555

Lysak RL, Hudson MK, Temerin M, Ion heating by strong electrostatic ion cyclotron turbulence, J. Geophys. Res. Space Phys. 85, 678-686 (1980). https://doi.org/10.1029/JA085iA02p00678

Mauk BH, Electromagnetic wave energization of heavy ions by the electric "phase bunching process, Geophys. Res. Lett. 9, 1163-1166 (1982). https://doi.org/10.1029/GL009i010p01163

Meeks Z, Simon S, Kabanovic S, A comprehensive analysis of ion cyclotron waves in the equatorial magnetosphere of Saturn, Planet. Space Sci. 129, 47-60 (2016). https://doi.org/10.1016/j.pss.2016.06.003

Meredith NP, Horne RB, Kersten T, Fraser BJ, Grew RS, Global morphology and spectral properties of EMIC waves derived from CRRES observations, J. Geophys. Res. Space Phys. 119, 5328-5342 (2014). https://doi.org/10.1002/2014JA020064

Mitchell DG, Kurth WS, Hospodarsky GB, Krupp N, Saur J, et al., Ion conics and electron beams associated with auroral processes on Saturn, J. Geophys. Res. Space Phys. 114, A02212 (2009). https://doi.org/10.1029/2008JA013621

Pandey RS, Pandey R, Srivastava AK, Karim S, Hariom, The electromagnetic ion-cyclotron instability in the presence of a.C. electric field for lorentzian kappa, Prog. Electromagn. Res. M. Pier M. 1, 207-217 (2008). https://doi.org/10.2528/PIERM08032601

Pandey RS, Singh DK, Study of electromagnetic ion-cyclotron instability in a magnetoplasma, Prog. Electromagn. Res. M. Pier M. 14, 147-161 (2010). https://doi.org/10.2528/PIERM10052501

Persoon AM, Gurnett DA, Kurth WS, Hospodarsky GB, Groene JB, et al., Equatorial electron density measurements in Saturn's inner magnetosphere, Geophys. Res. Lett. 32, L23105 (2005). https://doi.org/10.1029/2005GL024294

Rodríguez-Martínez M, Blanco-Cano X, Russell CT, Leisner JS, Wilson RJ, et al., Harmonic growth of ion-cyclotron waves in Saturn's magnetosphere, J. Geophys. Res. Space Phys. 115, A09207 (2010). https://doi.org/10.1029/2009JA015000

Rymer AM, Mauk BH, Hill TW, Paranicas C, Andr N, et al., Electron sources in Saturn's magnetosphere, J. Geophys. Res. Space Phys. 112, A02201 (2007). https://doi.org/10.1029/2006JA012017

Shukla NK, Singh D, Pandey RS, Analytical study of electromagnetic ion cyclotron wave for ring distribution with AC electric field in Saturn magnetosphere, https://iopscience.iop.org/issue/1742-6596/1817/1J. Phys. Conf. Ser. 1817, 012020 (2021). https://doi.org/10.1088/1742-6596/1817/1/012020

Sittler EC Jr, Ogilvie KW, Scudder JD, Survey of low-energy plasma electrons in Saturn's magnetosphere: voyagers 1 and 2, J. Geophys. Res. Space Phys. 88, 8847-8870 (1983). https://doi.org/10.1029/JA088iA11p08847

Smith EJ, Tsurutani BT, Saturn's magnetosphere: observations of ion cyclotron waves near the dione L shell, J. Geophys. Res. Space Phys. 88, 7831-7836 (1983). https://doi.org/10.1029/

JA088iA10p07831

Summers D, Ni B, Meredith NP, Timescales for radiation belt electron acceleration and loss due to resonant wave-particle interactions: 2. evaluation for VLF chorus, ELF hiss, and electromagnetic ion cyclotron waves, J. Geophys. Res. Space Phys. 112, A04207 (2007). https://doi.org/10.1029/2006JA011993

Summers D, Thorne RM, Relativistic electron pitch-angle scattering by electromagnetic ion cyclotron waves during geomagnetic storms, J. Geophys. Res. Space Phys. 108, 1143 (2003). https://doi.org/10.1029/2002JA009489

Szegö K, Glassmeier KH, Bingham R, Bogdanov A, Fischer C, et al., Physics of mass loaded plasmas, Space Sci. Rev. 94, 429-671 (2000). https://doi.org/10.1023/A:1026568530975

Thorne RM, Radiation belt dynamics: the importance of wave-particle interactions, Geophys. Res. Lett. 37, L22107 (2010). https://doi.org/10.1029/2010GL044990

Thorne RM, Summers D, Kinetic instability of a gyrating ring distribution with application to satellite pickup in planetary magnetospheres, Planet. Space Sci. 37, 535-544 (1989). https://doi.org/10.1016/0032-0633(89)90094-9

Usanova ME, Darrouzet F, Mann IR, Bortnik J, Statistical analysis of EMIC waves in plasmaspheric plumes from cluster observations, J. Geophys. Res. Space Phys. 118, 4946-4951 (2013). https://doi.org/10.1002/jgra.50464

Wilson RJ, Tokar RL, Henderson MG, Thermal ion flow in Saturn's inner magnetosphere measured by the Cassini plasma spectrometer: a signature of the Enceladus torus? Geophys. Res. Lett. 36, L23104 (2009). https://doi.org/10.1029/2009GL040225

Wu CS, Yoon PH, Freund HP, A theory of electron cyclotron waves generated along auroral field lines observed by ground facilities, Geophys. Res. Lett. 16, 1461-1464 (1989). https://doi.org/10.1029/GL016i012p01461

Young DT, Berthelier JJ, Blanc M, Burch JL, Bolton S, et al., Composition and dynamics of plasma in Saturn's magnetosphere, Science 307, 1262-1266 (2005). https://doi.org/10.1029/JA094iA05p05467101126/science1106151